vibration

MDPI

Article

Numerical Investigation of the Nonlinear Drill String Dynamics Under Stick–Slip Vibration

Mohammad Javad Moharrami [1], Hodjat Shiri [1,*] and Clóvis de Arruda Martins [2]

[1] Civil Engineering Department, Faculty of Engineering and Applied Science, Memorial University of Newfoundland, St. John's, NL A1B 3X5, Canada; mjmoharrami@mun.ca
[2] Offshore Mechanics Laboratory, Mechanical Engineering Department, Polytechnic School, University of São Paulo, São Paulo 05508-030, SP, Brazil; cmartins@usp.br
* Correspondence: hshiri@mun.ca

Abstract: This paper presents a comprehensive analysis of the influence of rotary table velocity, weight-on-bit, and viscous damping on the drill string stick–slip vibration. The analysis allows for studying the qualitative and quantitative variation of the dynamic response of the drill pipes and drill collars/bit. To achieve this goal, a robust and practical finite element (FE) model of the full-scaled drill string was developed based on a velocity-weakening formulation of the nonlinear bit–rock interaction. A detailed investigation of damping parameters was carried out. The performance of the developed model was verified through comparisons with a lumped-parameter model and a field test example. Parametric studies on the stick–slip response of the entire drill string under different field operational conditions were conducted. The dynamical time series of the system response were analyzed in terms of the phase planes, response spectra, and descriptive statistics of the drill pipes and drill collars. The findings of the study revealed that for a realistic drill string geometry, the angular velocity (i.e., mean, peak-to-peak amplitude, and standard deviation) and dominant frequency of self-excited torsional stick–slip oscillations along the drill pipes and drill collars/bit are mainly governed by the rotary table velocity. Furthermore, it was shown that the contribution of higher harmonics in the torsional stick–slip response of the drill pipes is more substantial than the drill collars/bit.

Keywords: drill string; stick–slip; nonlinear dynamic vibration; finite element modeling; Rayleigh viscous damping; parametric analysis

Citation: Moharrami, M.J.; Shiri, H.; Martins, C.d.A. Numerical Investigation of the Nonlinear Drill String Dynamics Under Stick–Slip Vibration. *Vibration* **2024**, *7*, 1086–1110. https://doi.org/10.3390/vibration7040056

Academic Editor: Evgeny Petrov

Received: 7 June 2024
Revised: 8 October 2024
Accepted: 10 November 2024
Published: 15 November 2024

1. Introduction

Drill string is an essential component of rotary drilling systems employed in onshore/offshore oil and gas extraction. A significant length of drill string is made of thin-walled drill pipes, which are loaded in tension and transfer the top rotary motion to the drill bit [1]. The lower end of the drill string is composed of various components, such as the thick-walled drill collars and stabilizers, collectively called the bottom-hole assembly (BHA) [2]. Drill collars are loaded in compression and provide the required axial force, known as weight-on-bit (WOB), to facilitate straight drilling [3]. Figure 1 shows an offshore drilling vessel and the basic components of the drill string.

Drill string is subjected to axial (i.e., bit bounce), lateral (i.e., whirl), and torsional (i.e., stick–slip) dynamic vibrations [4]. These vibrations can exist separately or coupled together in a linear or nonlinear manner [5]. Stick–slip vibration is a severe type of torsional oscillation, detrimental to the fatigue life of drill string and downhole equipment [6]. The primary cause of stick–slip vibration is the nonlinear friction at the bit–formation interface [1,5,7]. This type of vibration involves cyclic fluctuations in the bit angular velocity, ranging from zero up to more than twice the rotary table velocity [8]. The high angular velocities of the drill bit during the slip phase can induce severe axial and lateral

vibrations in the BHA, leading to excessive wear and even failure of the bit [9]. Furthermore, the high levels of torque-on-bit during the stick phase, varying between 500 and 10,000 Nm, can twist the drill string for several turns [1]. The consequent large torsional deformation during the twisting can cause failure of the drill pipes or threaded connections [2].

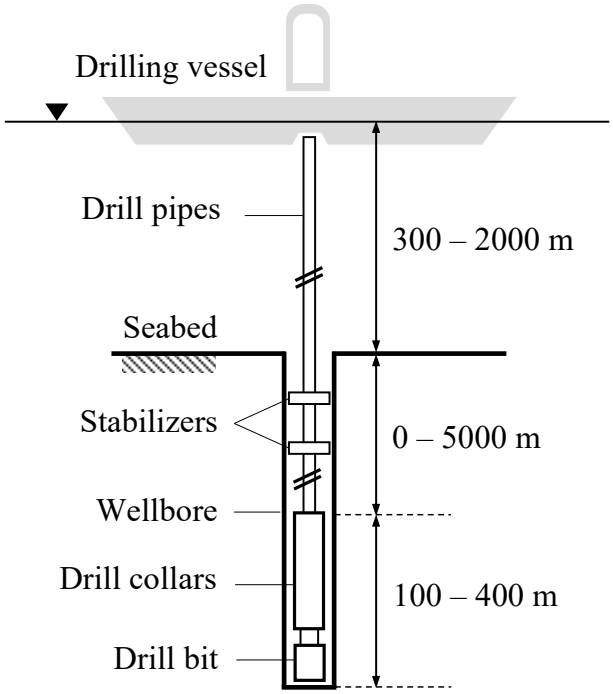

Figure 1. Schematic of a typical offshore drilling system.

Torsional vibration of drill string, either uncoupled or coupled with other vibration modes, has been extensively studied using (i) lumped-parameter models (e.g., [1,4,5,10–17]), (ii) continuous-parameter models (Cosserat theory of rods) (e.g., [18,19]), and (iii) finite element method (FEM) models (e.g., [9,14,20–22]). The influence of system parameters on the drill string vibrations has also been analyzed in a number of studies: Dareing and Livesay (1968) investigated the effect of rotary velocity, friction, and shock sub on the longitudinal vibration of the drill string [23]. The authors assumed a prescribed periodic motion at the bit in the absence of bit–rock excitation and contact forces. Liao et al. (2012) studied the influence of unbalanced mass, friction coefficient, and drive speed on the vibrations of a rotor–stator system [24]. Germay et al. (2009) analyzed the effect of weight-on-bit and rotational speed on the axial and torsional vibrations at the drill bit [22].

Although extensive literature has been dedicated to the dynamics of the drill string, the effects of field operating parameters on the torsional vibrations have not been extensively studied. Analyzing the vibrations under different operational conditions is essential for predicting the behavior of the entire system. It may also provide some valuable information about the influential external parameters in order to avoid harmful vibration modes and achieve a reliable and efficient drilling operation. Furthermore, the majority of the previous studies have analyzed the dynamics of the drill string through vibrations of the drill collars. Even though the drill collars have a significant influence on the overall dynamic response of the system, the behavior of the drill pipes as a slender structure has been less explored and is yet to be understood [19]. Therefore, the present paper aimed at comprehensive analyses of the stick–slip dynamics of the drilling assembly as an integrated system using an efficient integrated FEM model.

The objective of this paper was twofold. First, an integrated nonlinear numerical model was developed to obtain the dynamic response of the entire drill string under stick–slip vibration. A computationally efficient approach was used to model the rate-dependent bit–rock contact interface and capture the cutting and friction effects. The

nonlinear Timoshenko beam element was used to model the drill string, accounting for the shear deformation and the axial and torsional stiffness of the drill pipes and drill collars. The axial and torsional vibration modes were geometrically coupled, and the nonlinear effects of large rotation were taken into account. A linear perturbation frequency analysis was performed to estimate the eigenfrequencies of the drill string. The effect of energy dissipation due to the presence of the drill mud was incorporated along the drill pipes and drill collars using the Rayleigh viscous damping. A procedure was proposed for proper quantification of the Rayleigh damping coefficients to maintain the effect of higher vibration modes. The performance of the numerical model was compared with a five-degree-of-freedom lumped-parameter model and verified against the field test example of stick–slip.

Second, comprehensive dynamic analyses of the entire drill string under different operating conditions were carried out. The effects of rotary table velocity, weight-on-bit, and damping ratio on the torsional stick–slip vibration of the drill pipes and drill collars/bit were examined quantitatively and qualitatively. Due to the vital role of viscous damping in the overall response of the system, special attention was paid to the detailed analysis of damping. The spectral analyses were carried out to determine the effects of operating parameters on the stick–slip frequency of the system. The descriptive statistics, i.e., mean, amplitude, and standard deviation of angular velocities along the drill string, were computed for varying operational conditions.

The results showed that the amplitude, mean, and standard deviation of the angular velocities of the drill pipes and drill collars/bit under stick–slip occurrence were largely related to the rotary velocity and its threshold value. Also, the dominant frequency of stick–slip vibration was dependent on the rotary velocity, i.e., decreased with decreasing rotary velocity. The results indicated that the drill pipes can be excited at frequencies higher than the second natural vibration mode of the system with noticeable amplitudes.

The findings of the work were in good qualitative agreement with the field and experimental observations under stick–slip oscillation. The outcomes revealed new features of the overall torsional dynamics of the drill string as an integrated system.

2. Developing the FEM Model

A global three-dimensional FEM model of the drill string was developed in ABAQUS/Explicit. The overall configuration and material properties were taken from a drill string structure, as given in Table 1. The slenderness ratio (diameter divided by length) of less than 0.1 implies that the three-dimensional continuum drill string can be abstracted to a one-dimensional beam [25]. Therefore, the two-node linear interpolation beam element B31 (Timoshenko beam) was selected from the ABAQUS element library to model both the drill pipes and drill collars. The B31 is a one-dimensional line element in three-dimensional space that has stiffness associated with axial deformation, bending, and torsion [26]. Each node has six degrees of freedom: three translational and three rotational. Using the beam element in modeling the drill string can significantly reduce the computational cost yet provide a good approximation of the model response. As the tool joints have a negligible effect on the axial and torsional vibrations [27], the drill pipes were modeled with a uniform cross-sectional area. The effect of geometric nonlinearities, i.e., large rotational displacements and geometric coupling between the axial and torsional vibration modes, were taken into account. The consideration of geometric nonlinearities is vital in dynamics of structures and drill string systems [20,28,29]. Figure 2 shows the overall scheme of the modeled drill string, where x, y, and z are the translational degrees of freedom, whereas φ_x, φ_y, and φ_z are the rotational degrees of freedom around x, y, and z axes, respectively.

Table 1. Geometry and material properties of the drill string [1].

Parameter	Variable	Value	Unit
Drill pipe specification			
Drill pipe length	L_p	2000	m
Drill pipe outer diameter	D_p	0.1270	m
Drill pipe inner diameter	d_p	0.1086	m
Drill collar specification			
Drill collar length	L_c	150	m
Drill collar outer diameter	D_c	0.2286	m
Drill collar inner diameter	d_c	0.0762	m
Material specification			
Steel density	ρ	7850	kg/m^3
Young's modulus	E	2×10^{11}	N/m^2
Shear modulus	G	7.96×10^{10}	N/m^2

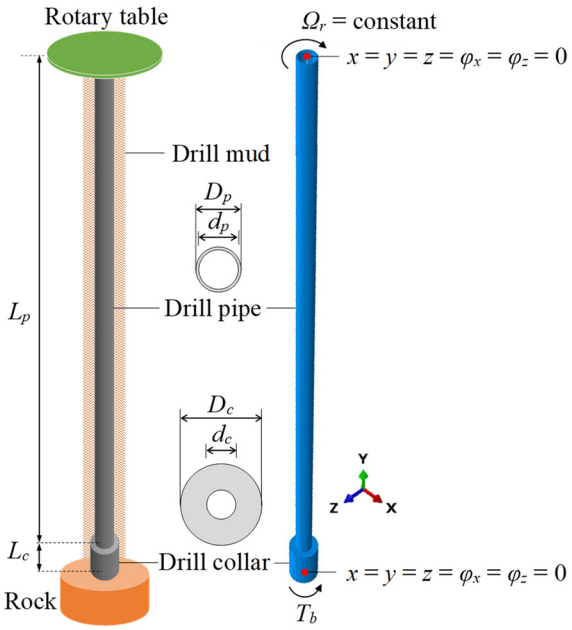

Figure 2. A sketch of the considered full drill string (**left**) and the corresponding FEM model developed in ABAQUS with boundary conditions at the surface and the bit (**right**).

2.1. Bit–Rock Contact Boundary Condition

Classically, for a static weight-on-bit, the bit–rock contact interface is characterized by a frictional torque decreasing with the bit angular velocity [30]. The nonlinear velocity-weakening behavior of the torque-on-bit has been observed in field and laboratory drilling experiments and is often considered the primary cause of the drill bit stick–slip oscillations [5,31,32].

ABAQUS/Explicit employs the kinematic and penalty contact models, in which the contact surfaces, i.e., the bit and the rock bodies, should be modeled through two- or three-dimensional finite elements. The inherent nonlinearity of the contact surfaces often leads to computational challenges and convergence issues. As an alternative approach to avoid the difficulties in contact analysis and efficiently employ the beam elements for minimizing the

computational cost, the frictional contact at the bit–rock interface was modeled through an equivalent frictional torque-on-bit T_b as follows:

$$T_b = \begin{cases} M, & if\ |M| < T_0\ \text{(stick mode)}, \\ M_{sl}, & otherwise\ \text{(slip mode)}. \end{cases} \quad (1)$$

where M is the magnitude of all the frictional moments acting on the bit (drill collar's end) about the longitudinal axis (tangent to the bit–rock contact surface), $T_0 = \mu_s R_b W_b$ is the break-away moment (maximum static friction torque), $M_{sl} = \mu(\dot{\varphi}_b) R_b W_b$ is the sliding friction moment about the longitudinal axis, R_b is the bit radius, $W_b > 0$ is the weight-on-bit, and $\mu(\dot{\varphi}_b)$ is the Static–Kinetic Exponential Decay friction formulation defined as follows:

$$\mu(\dot{\varphi}_b) = \left[\mu_c + (\mu_s - \mu_c) e^{-\gamma|\dot{\varphi}_b|}\right] \quad (2)$$

where $\dot{\varphi}_b = \Omega_b$ is the bit angular velocity, μ_c and μ_s are the kinetic (Coulomb) and static friction coefficients, respectively, and $\gamma > 0$ is the constant decay coefficient. It is noted that μ_s can be greater than one depending on the surfaces, while $\mu_c \in (0, 1)$ and $\mu_s > \mu_c$.

The drill string was uniformly discretized with 64 elements on the pipe section and 32 elements on the collar section. The number of elements was selected based on a mesh sensitivity analysis, which verified convergence of the numerical results for the entire drill string.

2.2. Eigenfrequency Extraction

The stationary behavior of the rotating drill string is equivalent to the dynamics of the same structure fixed at the surface and free at the bit [33]. Therefore, the boundary condition at the upper end (rotary table) was completely fixed, while the lower end (bit) was only free to rotate about the longitudinal axis of the string.

The first 500 undamped natural frequencies of the drill string with the specified boundary conditions were extracted using the Lanczos linear perturbation method [26]. The criterion for extracting 500 natural modes was to obtain at least ten natural torsional frequencies of the drill string. The obtained natural frequencies are given in Table 2, where $\omega = 2\pi f$.

Table 2. Torsional natural frequencies of the drill string.

Mode Number	Natural Frequency	Natural Frequency
n	f_n (Hz)	ω_n (rad/s)
1	0.19	1.21
2	0.84	5.26
3	1.60	10.02
4	2.37	14.88
5	3.14	19.75
6	3.92	24.62
7	4.69	29.48
8	5.46	34.33
9	6.23	39.16
10	7.04	44.22

2.3. Viscous Damping Effect

The viscous damping due to the drill mud is an important aspect of the drill string dynamics. Increasing the torsional damping can disfavor the stick–slip oscillation [1,34,35] and extend the upper boundary of the stable operating region of the drill string [36–39].

Therefore, the inclusion of viscous damping effects is essential for realistic modeling and satisfactory results.

In the present paper, the frequency-dependent Rayleigh damping was used to model the mud viscous damping in the FEM simulations. The standard form of Rayleigh damping is defined as a linear combination of the mass M and stiffness K matrices as follows [40,41]:

$$C = \alpha M + \beta K \tag{3}$$

where α and β are the mass and stiffness proportional coefficients, respectively. The damping ratio for mode n of the system is given by the following [41]:

$$\xi_n = \frac{\alpha}{2\omega_n} + \frac{\beta\omega_n}{2} \tag{4}$$

where ω_n (rad/s) is the natural frequency of mode n. The coefficients α and β can be determined from two specified modal damping ratios, i.e., ξ_i and ξ_j. Rewriting Equation (4) in matrix form for the specified modes leads to a set of two algebraic equations as follows:

$$\frac{1}{2}\begin{bmatrix} 1/\omega_i & \omega_i \\ 1/\omega_j & \omega_j \end{bmatrix}\begin{Bmatrix} \alpha \\ \beta \end{Bmatrix} = \begin{Bmatrix} \xi_i \\ \xi_j \end{Bmatrix} \tag{5}$$

Assuming $\xi_i = \xi_j = \xi$ in Equation (5), the coefficients α and β can be computed as follows:

$$\alpha = \xi\frac{2\omega_i\omega_j}{\omega_i + \omega_j}, \quad \beta = \xi\frac{2}{\omega_i + \omega_j} \tag{6}$$

For a drill string with many modes over a large range of natural frequencies, the Rayleigh method can result in damping ratios significantly different than the target modal damping. Therefore, the natural frequencies ω_i and ω_j should be chosen to ensure that the damping ratios over the intermediate modes are close to the target damping. A preliminary investigation was conducted to determine ω_i and ω_j for which the variation of the damping ratio over the intermediate modes was minimized. To achieve $\xi = 0.02$, for example, ω_i was set to be the first natural frequency ω_1, whereas ω_j was set to be about the second, the third, the fifth, and the tenth natural frequency of the system. Figure 3 shows the variation of Rayleigh damping over the selected frequency bands.

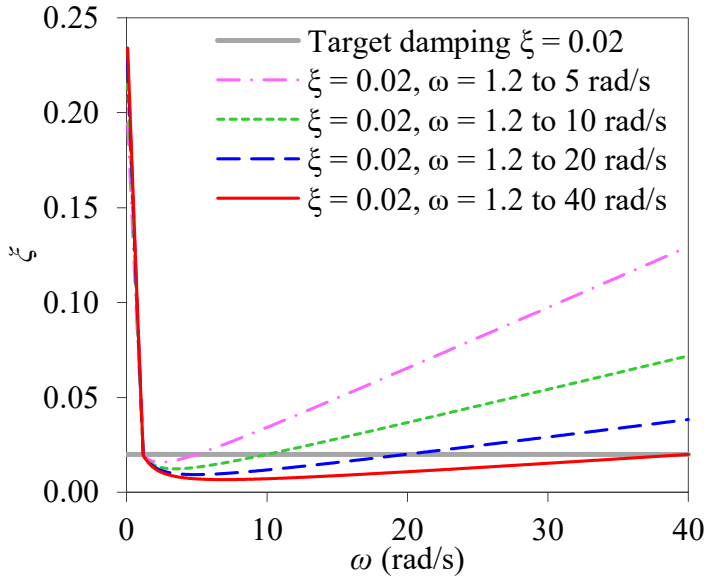

Figure 3. Effect of frequency band on the Rayleigh damping variations.

The results indicated that under a narrow frequency band, i.e., ω_i =1.2 rad/s = ω_1 and ω_j = 5 rad/s ≈ ω_2, the damping ratios for higher modes were immensely larger than the target damping, the so-called de-amplification effect. However, under the wider frequency bands, i.e., ω_i = 1.2 rad/s = ω_1 and ω_j = 40 rad/s ≈ ω_{10}, the damping ratios for higher modes were smaller than the target damping. Therefore, in the rest of this paper, α and β were calculated using $\omega_i = \omega_1$ and $\omega_j = \omega_{10}$ (see Tabe 2) in order to minimize the frequency-dependent damping variations and maintain the high-frequency torsional vibrations reported in the previous studies (e.g., [22,42]). This broad frequency band gave a conservative underdamped system for intermediate modes, which is more favorable than a non-conservative overdamped system, particularly in fatigue assessment of the drill string system.

3. Comparison and Verification of the Models

3.1. Comparison of the FEM Model with a Lumped-Parameter Model

A five-degree-of-freedom lumped-parameter model was developed based on the generic lumped-parameter model of Navarro-Lopez and Cortes (2007) [11] to make comparisons with the FEM model; see Figure 4. The key assumptions of the model are as follows: (i) the drill pipes behave as torsional spring without structural damping; the drill collars behave as a rigid body, (ii) the frictional contact in the pipe threaded connections and at the pipe–borehole interface is ignored, (iii) the energy dissipation effect of the drilling mud is modeled by lumped viscous damping, (iv) the motor dynamic is not considered, (v) the rotary table is massless; the rotary velocity is constant, and (vi) the weight-on-bit is constant. The corresponding set of motion equations are as follows:

$$\begin{cases} k_p(\varphi_r - \varphi_1) - T_r = 0 \\ J_p\ddot{\varphi}_1 + c_p\dot{\varphi}_1 + k_p(\varphi_1 - \varphi_r) + k_p(\varphi_1 - \varphi_2) = 0 \\ J_p\ddot{\varphi}_2 + c_p\dot{\varphi}_2 + k_p(\varphi_2 - \varphi_1) + k_p(\varphi_2 - \varphi_3) = 0 \\ J_p\ddot{\varphi}_3 + c_p\dot{\varphi}_3 + k_p(\varphi_3 - \varphi_2) + k_p(\varphi_3 - \varphi_b) = 0 \\ J_b\ddot{\varphi}_b + c_b\varphi_b + k_p(\varphi_b - \varphi_3) + T_b = 0 \end{cases} \quad (7)$$

where φ_r, φ_1, φ_2, φ_3, and φ_b are the angular displacements of the rotary table, drill pipe 1, drill pipe 2, drill pipe 3, and drill collars/bit, respectively, $T_r = k_p(\phi_r - \phi_1)$ is the torque delivered by the rotary table to the drill string ($T_r > 0$), and T_b is a nonlinear function representing the frictional torque-on-bit. The model parameters were calculated as follows:

$$J_p = \rho I_p(L_p/4), \quad J_c = \rho I_c L_c, \quad J_b = J_c + J_p/2, \quad k_p = GI_p/(L_p/4) \quad (8)$$

with

$$I_p = (\pi/32)\left(D_p^4 - d_p^4\right), \quad I_c = (\pi/32)\left(D_c^4 - d_c^4\right) \quad (9)$$

where J_p, J_c, and J_b, are the mass moment of inertia of the drill pipe, drill collar, and drill bit, respectively, k_p is the torsional stiffness of the drill pipe, and I_p and I_c are the polar moment of inertia of the pipe and the collar sections, respectively. The equivalent viscous damping coefficient of the drill pipe (c_p) and drill collar/bit (c_b) were calculated as follows:

$$c_p = \hat{c}(L_p/4), \quad c_b = \hat{c}(L_p/8) \quad (10)$$

where $\hat{c}$ is the viscous damping coefficient per unit length of the drill pipe.

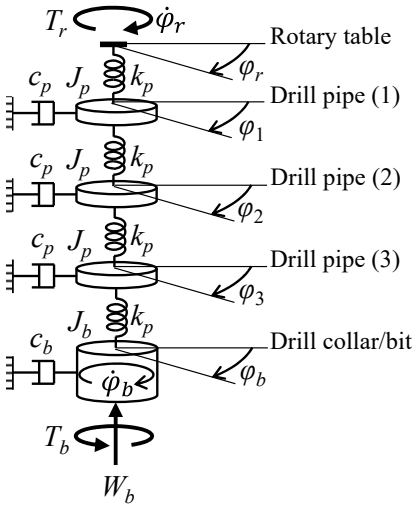

Figure 4. Lumped-parameter model representation of the drill string.

The frictional torque-on-bit T_b was modeled as a combination of the Karnopp (1985) model [43] and the Stribeck effect (negatively sloped friction at the slip phase) through a variable structure proposed by Sepehri et al. (1996) [44], Leine et al. (1998) [45], and Navarro-Lopez and Cortes (2007) [11], as illustrated in Figure 5. Thus,

$$T_b = \begin{cases} T_{st}\,, if\ |\dot{\varphi}_b| < V_d\ \ and\ |T_{st}| \le T_0\ \text{(stick mode)}, \\ T_0 sgn(T_{st})\,, if\ |\dot{\varphi}_b| < V_d\ \ and\ |T_{st}| > T_0\ \text{(transition from stick to slip)}, \\ T_{sl} sgn\left(\dot{\varphi}_b\right),\ if\ |\dot{\varphi}_b| \ge V_d\ \text{(slip mode)}. \end{cases} \tag{11}$$

with

$$T_{st} = -c_b\dot{\varphi}_b - k_p(\varphi_b - \varphi_3),\ T_0 = \mu_s R_b W_b,\ T_{sl} = \mu\left(\dot{\varphi}_b\right) R_b W_b \tag{12}$$

where $V_d > 0$ is the threshold velocity, T_{st} is the reaction torque during the stick phase that must overcome the break-away torque to make the bit move, T_0 is the break-away torque (maximum static friction torque), T_{sl} is the sliding friction torque, R_b is the bit radius, $W_b > 0$ is the weight-on-the bit, and $\mu\left(\dot{\varphi}_b\right)$ is the bit exponential-decay friction coefficient defined in Equation (2). The exponential decaying behavior of the torque-on-bit (Stribeck effect) is in agreement with the field and experimental observations [5,31,32].

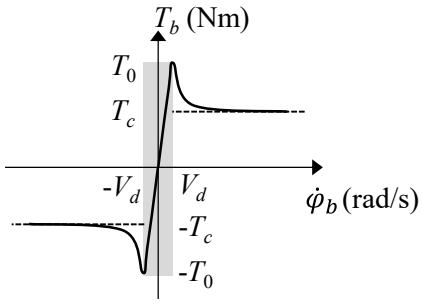

Figure 5. Friction model at the bit: switch friction model (enhanced Karnopp friction model) + Stribeck model.

The drill string vibration obtained from the numerical model was compared with the lumped-parameter model to have a comparative evaluation of the models' performance. The simulations were carried out for Ω_r = 7.33 rad/s (7.33 × 60/2π = 70 rpm), which is within the common field operating range, W_b = 40 kN, and ξ = 0.03.

The model parameters are given in Table 3. The equations of motion, Equations (6) and (11), were numerically integrated using the 4th–5th order Runge–Kutta method with variable time steps through the built-in function 'ode45' in MATLAB. The initial condition for all of

the state variables (except Ω_r) was taken as zero. To achieve $\xi = 0.03$, the viscous damping coefficient per unit length of drill pipes $\hat{c} = 0.0378$ Ns/rad adapted from Jansen and van den Steen (1995) [1] was used.

Table 3. Model parameters computed for the full drill string configuration given in Table 1.

Quantity	Variable	Value	Unit
Mass moment of inertia of drill pipe	J_p	46.6438	kgm^2
Mass moment of inertia of bit	J_b	335.1180	kgm^2
Torsional stiffness of drill pipe	k_p	1891.8971	Nm/rad
Equivalent viscous damping coefficient for drill pipe	c_p	18.9	Nms/rad
Equivalent viscous damping coefficient for drill collars/bit	c_b	9.45	Nms/rad
Bit–rock interface parameters [11]			
Bit outer diameter	D_b	0.311 (12¼)	m (inch)
Bit radius	R_b	0.1555	m
Static friction coefficient	μ_s	0.8	–
Kinetic (Coulomb) friction coefficient	μ_c	0.5	–
Decay coefficient	γ	0.9	–
Threshold velocity	V_d	1×10^{-6}	–

Figure 6 shows the stick–slip response of the drill string obtained from the FEM and lumped-parameter models. There is a good agreement between the results. Also, the limit cycling behavior is in agreement with field and experimental measurements [1,46].

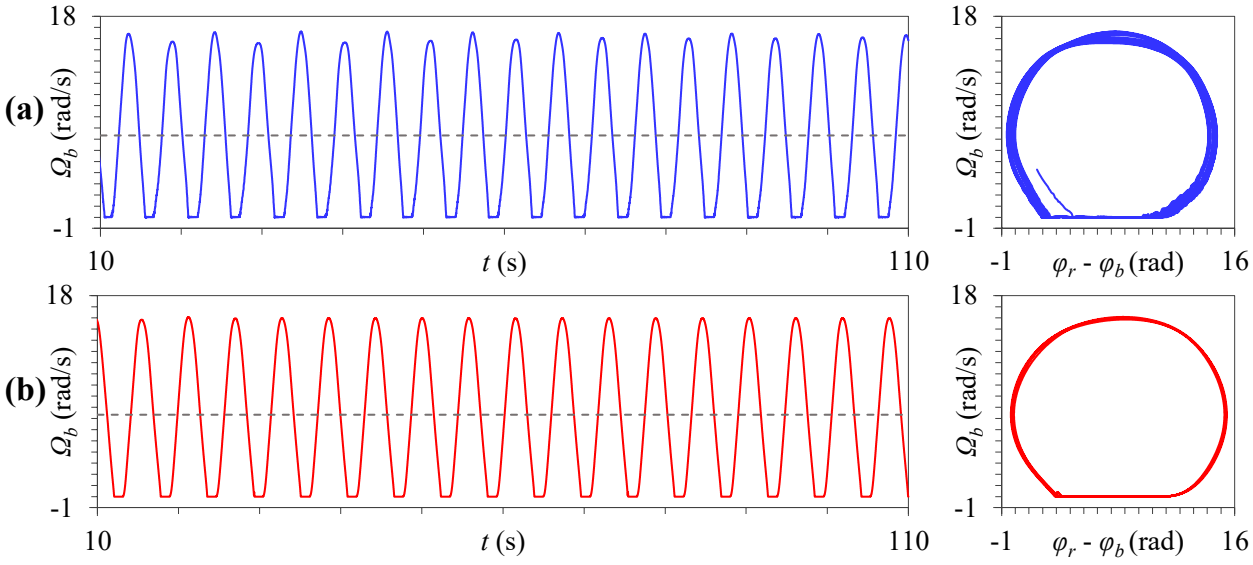

Figure 6. Example stick–slip time series and phase planes of the bit angular velocity obtained from (**a**) the FEM model and (**b**) the lumped-parameter model using Equations (7) and (11) with parameter values given in Table 3. $\Omega_r = 7.33$ rad/s (dashed lines), $W_b = 40$ kN, and $\xi = 0.03$ (with $\alpha = 0.070416$ 1/s and $\beta = 0.00132142$ s).

3.2. Field Test Verification

The FEM and lumped-parameter models developed in this paper were verified against field test data published in Kyllingstad and Nessjøen (2009) [47]. A realistic drill string of about 3200 m long consisting of 3100 m drill pipe and 100 m BHA was modeled based on the numerical and analytical procedures presented in Sections 2 and 3.1, respectively. Figure 7 shows the result of the comparison. Although differences were observed, a fairly good match was achieved between the simulation results and the field test, which verifies the performance of the developed models under stick–slip vibration. It is noted that the difference between simulation results and the field test may be related to the bit–rock interface parameters [48]. Due to the lack of availability of drilling parameters at the bit–rock interface, these parameters were obtained from other studies (e.g., [11]). A better agreement between the simulation results and the field test can be obtained if the bit–rock-related parameters are validated based on downhole field measurements.

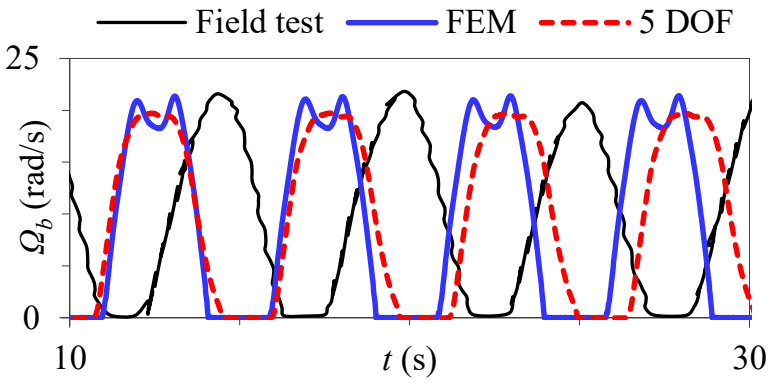

Figure 7. Example of stick–slip vibration occurring in the field test under constant rotational velocity Ω_r = 9.42 rad/s. Field test result from [48].

4. Results and Discussion

The numerical model developed in Section 2 was used for parametric studies. The values of rotary table velocity Ω_r, weight-on-bit W_b, and damping ratio ξ were varied to investigate their effects on the dynamics of the drill string and the existence of stick–slip. Only one variable was changed at each simulation to assess its individual influence. The time series of angular velocities were obtained for observation nodes along the drill string over 110 s for which the drill string exhibits steady-state stick–slip vibrations. The first 10 s of the analysis was the ramping-up of the rotary velocity from zero to the desired level, which is not displayed in the time series.

For each simulation, the peak-to-peak angular velocities of the observation nodes were calculated from t = 70 s to t = 90 s. Figure 8 demonstrates the response amplitude of the drill pipe mid-point (1150 m above the bit) and the drill bit under stick–slip oscillations. The observed torsional oscillations of the drill string under stick–slip conditions were limit cycles (bounded periodic vibrations). Therefore, the considered time duration covered at least one full cycle of the velocity oscillation for each node, and the calculated amplitudes represented the absolute amplitude of the whole simulation for that node. Furthermore, the apparent oscillations of the peak-to-peak velocities under stick–slip situation were negligible and did not significantly affect the calculated amplitudes; see Figure 8. The statistical properties of the system response, such as mean and standard deviation of the angular velocities, were then evaluated at each node throughout the time series from t = 10 s to t = 110 s. Adequate quantification of the statistical characteristics can be further used in fatigue analysis of the drill string system.

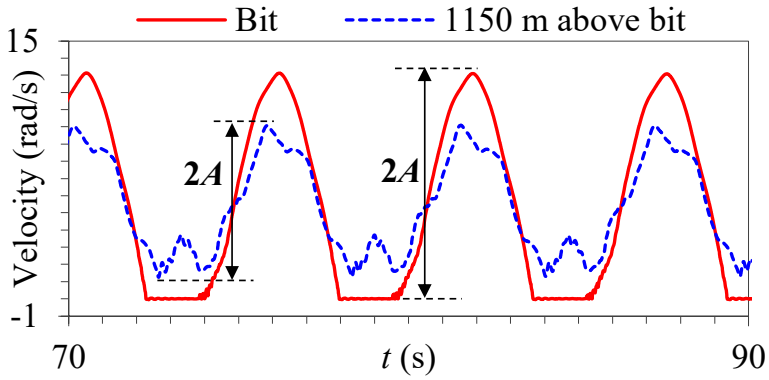

Figure 8. Definition of the peak-to-peak amplitude ($2A$) of angular velocity under stick–slip conditions for Ω_r = 5.24 rad/s, ξ = 0.03, and W_b = 40 kN.

To gain more in-depth insight into the behavior of the drill string under steady-state stick–slip vibration, the frequency analyses of the numerically obtained angular velocities were carried out. The time series of angular velocities along the drill string were treated using the fast Fourier transform (FFT). The obtained spectra indicated the discrete frequencies and amplitudes of the angular velocities that contributed to the stick–slip response of the system. The time series from t = 10 s to t = 110 s were sampled at a frequency of 80 Hz (Nyquist frequency 40 Hz) to achieve high-resolution spectra. The resolution of the obtained spectra was 0.01 Hz; therefore, the results were quantitative representations of the contributing frequencies. It is worth noting that the amplitudes of zero frequency components of the response spectra correspond to twice the mean angular velocities, which are not represented in the plots. Also, it is noted that the ordinate in each spectrum plot represents the normalized amplitude; that is, the amplitude of each frequency divided by the amplitude of the dominant frequency.

4.1. Effect of Rotary Velocity Ω_r

Four different levels of Ω_r were considered: 2.09, 5.24, 7.33, and 11.52 rad/s. The W_b and ξ were fixed at 40 kN and 0.03, respectively, with α = 0.070416 1/s and β = 0.00132142 s.

Figures 9 and 10 show the time series and the corresponding phase planes of angular velocity at the bit and a drill pipe located 1900 m above the bit, respectively, under varying Ω_r. For Ω_r smaller than a particular threshold value, i.e., 2.09, 5.24, and 7.33 rad/s, the drill bit undergoes periodic stick–slip vibration, whereas the drill pipe experiences regular periodic torsional vibration; see plots (a)–(c) in Figures 9 and 10 This situation can be identified by the closed trajectories of the phase planes representing the ceaseless torsional oscillations. As Ω_r increases up to a certain threshold value, the duration of the stick phase at the bit is decreased, while the amplitude of the vibration at both the drill pipe and bit is increased. This agrees with field and experimental observations (e.g., [47,49]). For higher values of Ω_r, i.e., 11.52 rad/s, which exceed the threshold value, the torsional vibrations at both the bit and drill pipe gradually damp out, and the drill string performs at stable condition with a velocity close to the rotary velocity; see plot (d) in Figures 9 and 10. The suppression of stick–slip oscillation by increasing the rotary velocity beyond the threshold value is in agreement with field observations (e.g., [1,34,47]).

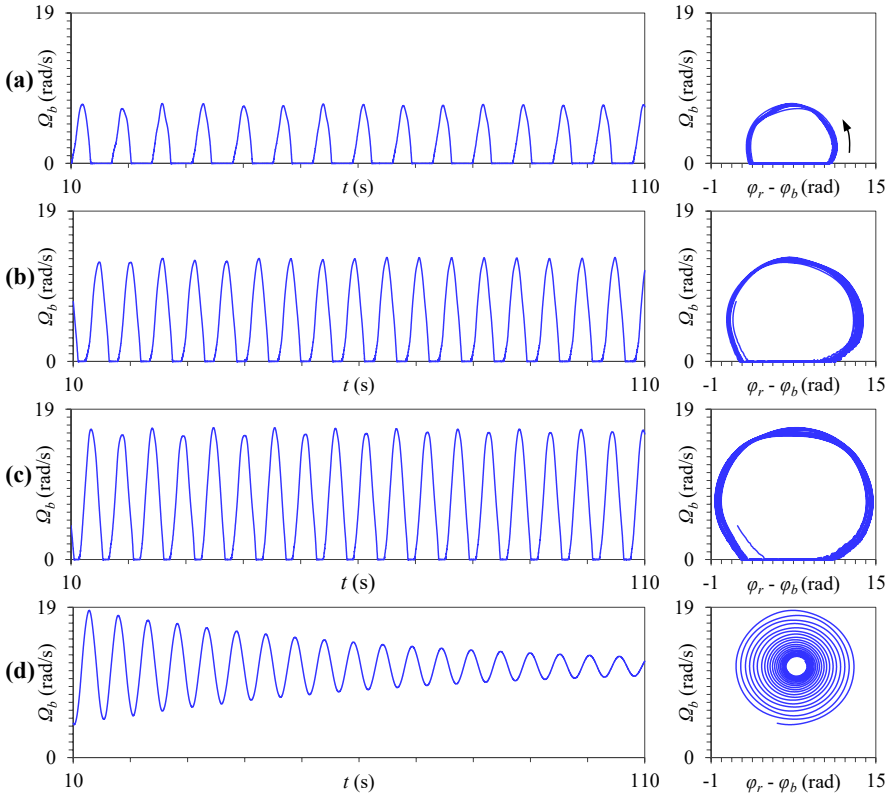

Figure 9. Time series and phase planes of the angular velocity at the drill bit for W_b = 40 kN, ξ = 0.03, and Ω_r of (**a**) 2.09, (**b**) 5.24, (**c**) 7.33, and (**d**) 11.52 rad/s.

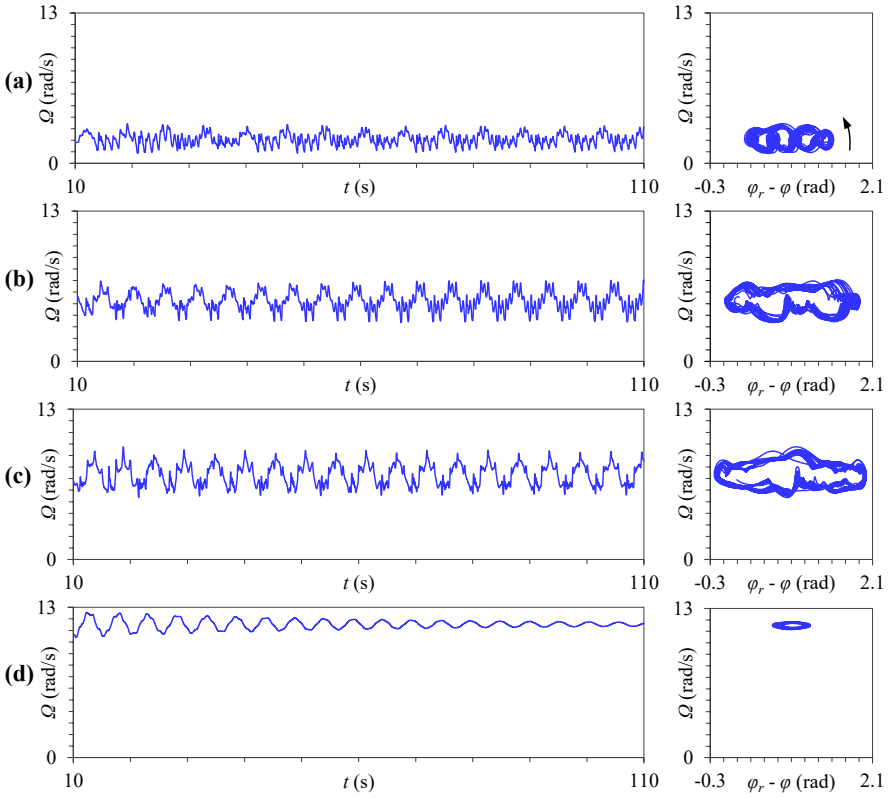

Figure 10. Time series and phase planes of the angular velocity at 1900 m above the drill bit for W_b = 40 kN, ξ = 0.03, and Ω_r of (**a**) 2.09, (**b**) 5.24, (**c**) 7.33, and (**d**) 11.52 rad/s.

Table 4 presents the calculated mean angular velocities along the drill string for varying Ω_r. Under each Ω_r, the mean angular velocities of the drill pipes and drill collars along the drill string are in the vicinity of the rotary velocity. This indicates that the mean velocity of the drill string is directly related to the rotary velocity at the surface.

Table 4. Mean angular velocity μ (rad/s) at different points along the drill string for W_b = 40 kN, ξ = 0.03, and varying Ω_r.

Distance Above the Bit (m)	Ω_r = 2.09 rad/s	Ω_r = 5.24 rad/s	Ω_r = 7.33 rad/s	Ω_r = 11.52 rad/s
2150	2.09	5.24	7.33	11.52
1900	2.10	5.23	7.33	11.52
1650	2.10	5.21	7.32	11.51
1400	2.11	5.20	7.32	11.51
1150	2.11	5.19	7.31	11.50
900	2.12	5.18	7.31	11.50
650	2.12	5.16	7.31	11.50
400	2.13	5.15	7.30	11.49
150	2.14	5.15	7.30	11.49
112.5	2.14	5.15	7.30	11.49
75	2.14	5.15	7.30	11.49
37.5	2.14	5.15	7.30	11.49
0	2.14	5.15	7.30	11.49

Figure 11 presents the amplitude spectra of angular velocities at the drill bit and a drill pipe located 1900 m above the bit under stick–slip vibration for different Ω_r. For low levels of Ω_r, i.e., 2.09 rad/s, the dominant frequencies of both the bit and drill pipe f_D = 0.14 Hz are considerably smaller than the first torsional natural frequency of the system f_1 = 0.19 Hz, f_D/f_1 = 0.73; see Figure 11a. This indicates that stick–slip vibration can occur at frequencies lower than the first natural frequency of the drill string. This is an interesting finding that agrees with published field observations [47]. For higher Ω_r, i.e., 5.24 and 7.33 rad/s, the dominant frequencies of both the bit and drill pipe f_D = 0.18~0.19 Hz are slightly smaller than the first torsional natural frequency of the system; see Figure 11b,c. The difference between the dominant frequencies and the first natural frequency of the system is associated with the nonlinear frictional torque due to the bit–rock interaction.

According to Figure 11a–c, the amplitude decreases with frequency at the drill bit; that is, the higher harmonics have a smaller contribution to the stick–slip vibration of the drill collars/bit, especially for higher Ω_r. In contrast, the contribution of higher harmonics is significant in the drill pipes, especially for lower Ω_r. For instance, in Figure 11a, corresponding to the drill pipe at 1900 m above the bit, the peak frequencies are 0.29, 0.86, 1.58, and 2.44 Hz, which the latter three are related to the second (0.838 Hz), third (1.595 Hz), and fourth (2.368) natural torsional frequency of the system, respectively; see Table 2**.** From these results, it can be concluded that under a stick–slip vibration, the contribution of higher frequencies in the response of the drill pipes is more noticeable than that in the drill collars/bit. This can be related to the smaller cross-sectional area and longer length of the drill pipe section compared to the drill collar section.

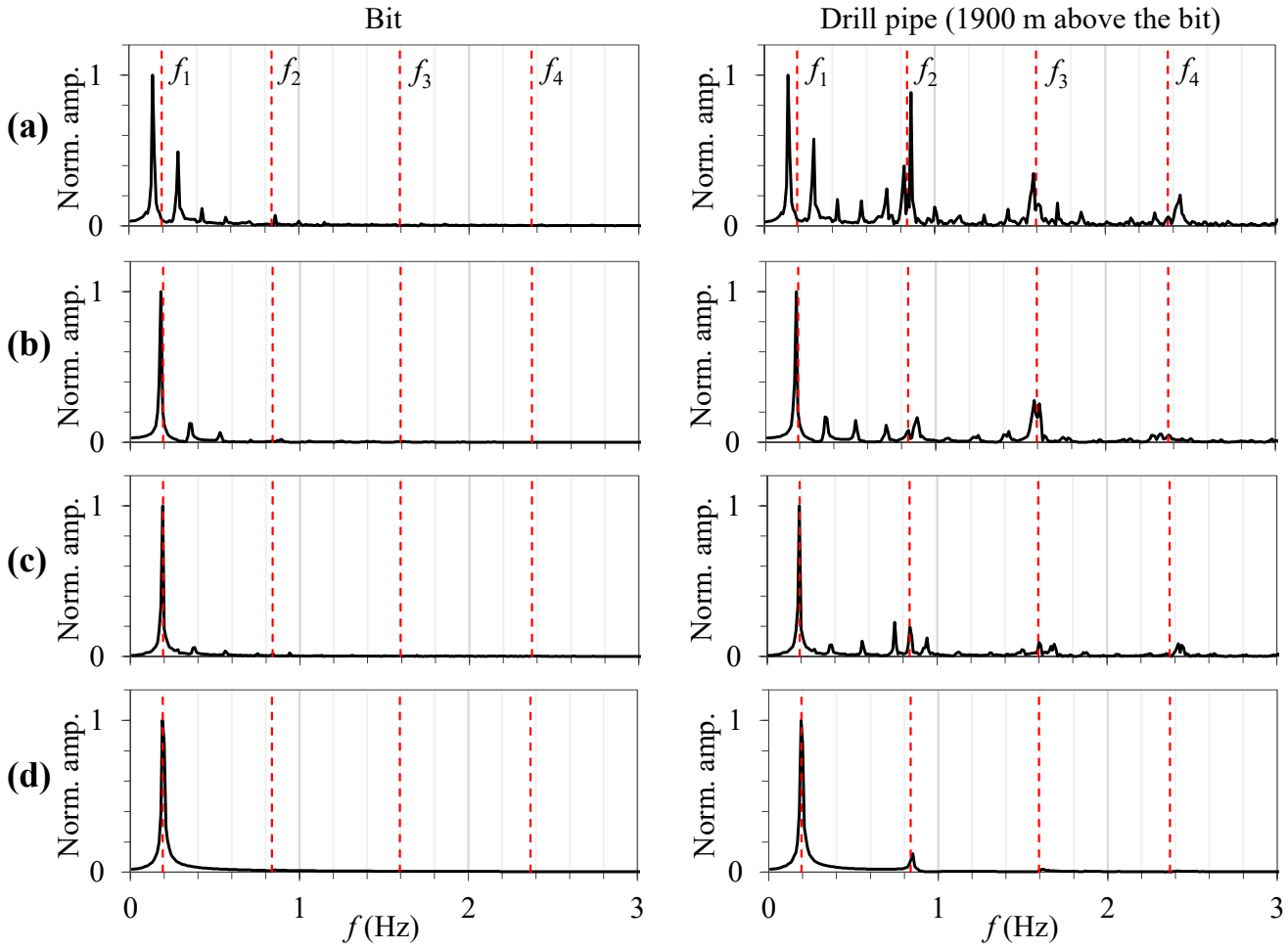

Figure 11. Response spectra of angular velocity at the drill bit (**left**) and 1900 m above the bit (**right**) with W_b = 40 kN, ξ = 0.03, and Ω_r of (**a**) 2.09, (**b**) 5.24, (**c**) 7.33, and (**d**) 11.52 rad/s. Dashed lines indicate natural frequencies.

4.2. Effect of Weight-on-Bit W_b

Simulations were carried out using four different values of W_b: 10, 30, 40, and 50 kN. The Ω_r and ξ were considered to be fixed at 6.3 rad/s and 0.03, respectively, with α = 0.070416 1/s and β = 0.00132142 s.

Figures 12 and 13 show the time series and the corresponding phase planes of angular velocity at the bit and a drill pipe located 1650 m above the bit, respectively, for varying W_b. For levels of W_b smaller than a certain threshold value, i.e., 10 kN, no stick–slip vibration is observed, and the torsional vibrations at both the bit and drill pipe gradually disappear; see plot (a) in Figures 12 and 13. As the W_b increases and exceeds the threshold value, i.e., 30, 40, and 50 kN, the drill bit exhibits periodic stick–slip vibration, resulting in periodic torsional vibration at the drill pipe; see plots (b)–(d) in Figures 12 and 13. This indicates that increasing the W_b can give rise to more severe stick–slip vibration with a larger amplitude, whereas decreasing the W_b can diminish the stick–slip condition. This is in accordance with field measurement data (e.g., [5]).

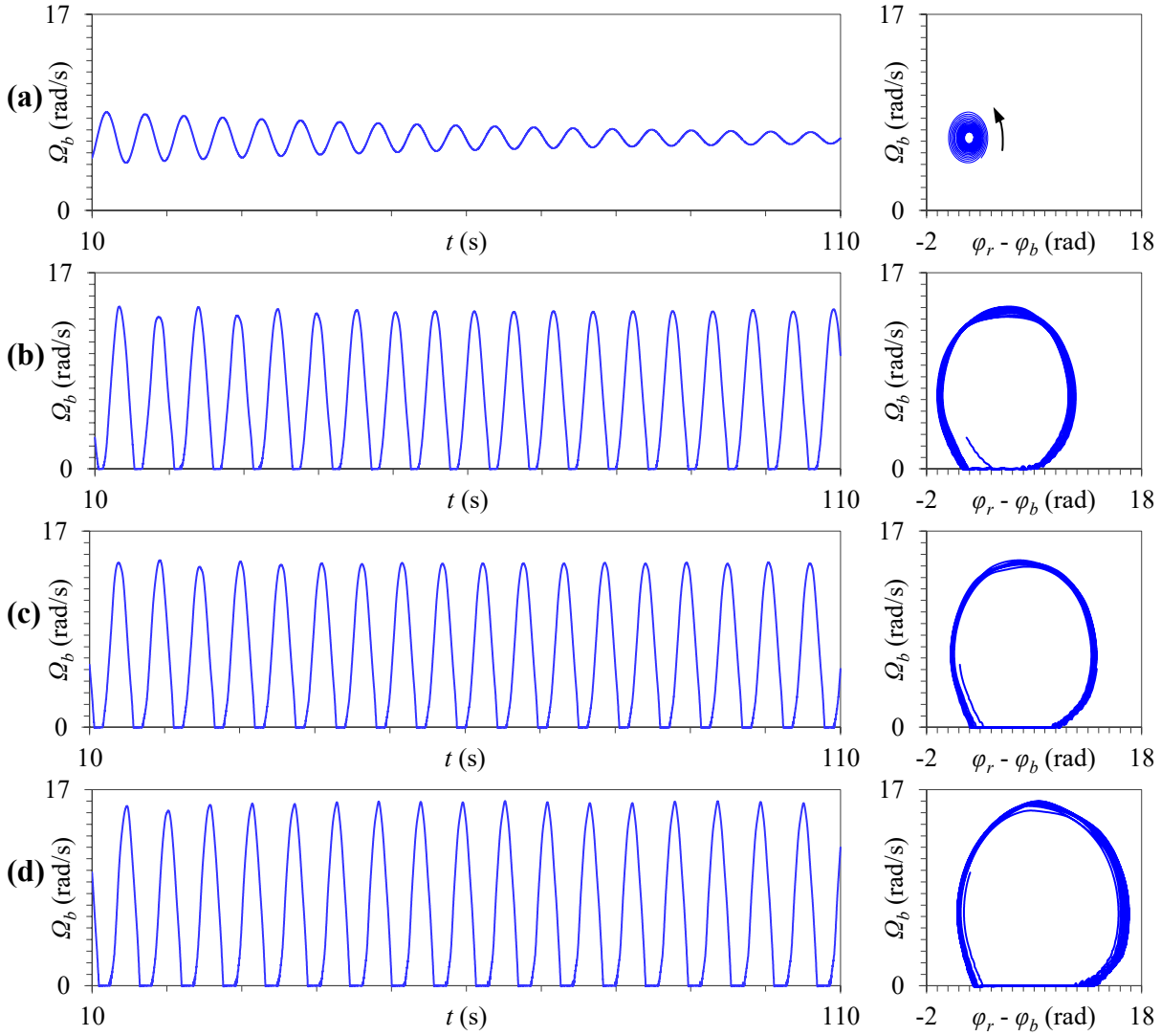

Figure 12. Time series and phase planes of the angular velocity at the bit for Ω_r = 6.3 rad/s, ξ = 0.03, and W_b of (**a**) 10, (**b**) 30, (**c**) 40, and (**d**) 50 kN.

The increase in W_b is associated with a rise in the break-away torque, $T_0 = \mu_s R_b W_b$, which is accompanied by a prolonged stick phase and a larger slip amplitude. This can be described in terms of the physical phenomenon as follows: if the weight-on-bit is increased, it will produce a greater frictional torque that needs to be overcome in order to enter the slip phase. This, in turn, requires a larger twisting of the drill string to accumulate reaction torque in the bit until it reaches the frictional torque. Therefore, the duration of the stick phase under fully developed stick–slip condition is more extended for larger W_b; see Figure 12b–d.

Table 5 shows the calculated mean angular velocity along the drill string. For small levels of W_b with no stick–slip vibration, i.e., W_b = 10 kN, the mean angular velocity of the entire drill string is equal to the rotary velocity. As the W_b increases and exceeds the threshold value, the mean angular velocity along the drill string becomes different from the rotary velocity. The difference between the rotary velocity and the mean angular velocity along the drill string indicates a continuous twist and, thus, torsional instability in the drill string during stick–slip vibration.

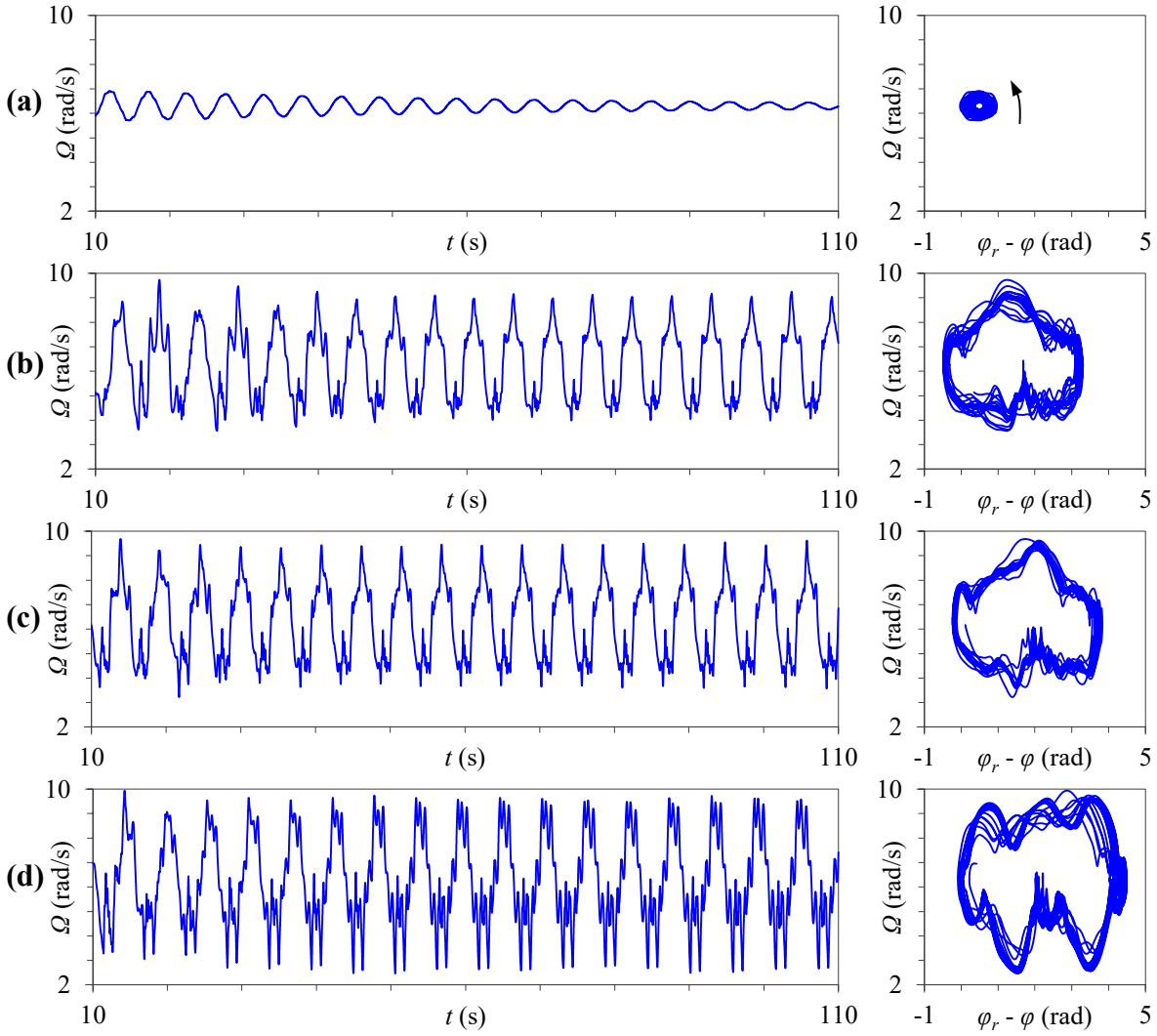

Figure 13. Time series and phase planes of the angular velocity at 1650 m above the bit for Ω_r = 6.3 rad/s, ξ = 0.03, and W_b of (**a**) 10, (**b**) 30, (**c**) 40, and (**d**) 50 kN.

Table 5. Mean angular velocity μ (rad/s) at different points along the drill string for Ω_r = 6.3 rad/s, ξ = 0.03, and varying W_b.

Distance Above the Bit (m)	W_b = 10 kN	W_b = 30 kN	W_b = 40 kN	W_b = 50 kN
2150	6.3000	6.3000	6.3000	6.3000
1900	6.3010	6.3024	6.2816	6.2807
1650	6.3020	6.3048	6.2631	6.2619
1400	6.3029	6.3072	6.2450	6.2441
1150	6.3038	6.3096	6.2282	6.2274
900	6.3047	6.3119	6.2129	6.2117
650	6.3055	6.3142	6.1986	6.1968
400	6.3062	6.3164	6.1853	6.1826
150	6.3069	6.3185	6.1728	6.1694
112.5	6.3069	6.3185	6.1727	6.1693
75	6.3069	6.3185	6.1726	6.1692
37.5	6.3069	6.3185	6.1726	6.1692
0	6.3069	6.3185	6.1726	6.1693

Figure 14 illustrates the response spectra of the angular velocities for varying W_b. According to this figure, for different levels of W_b, the stick–slip dominant frequency f_D~0.19 Hz remains close to the first torsional natural frequency of the system 0.19188 Hz. This implies that the dominant frequency is independent of W_b. It is noted that increasing W_b has been shown to increase the frequency of the stick–slip limit cycle depending on the operating parameter [22]. Moreover, it is observed that larger W_b can excite higher frequency components in the drill pipes; see Figure 14.

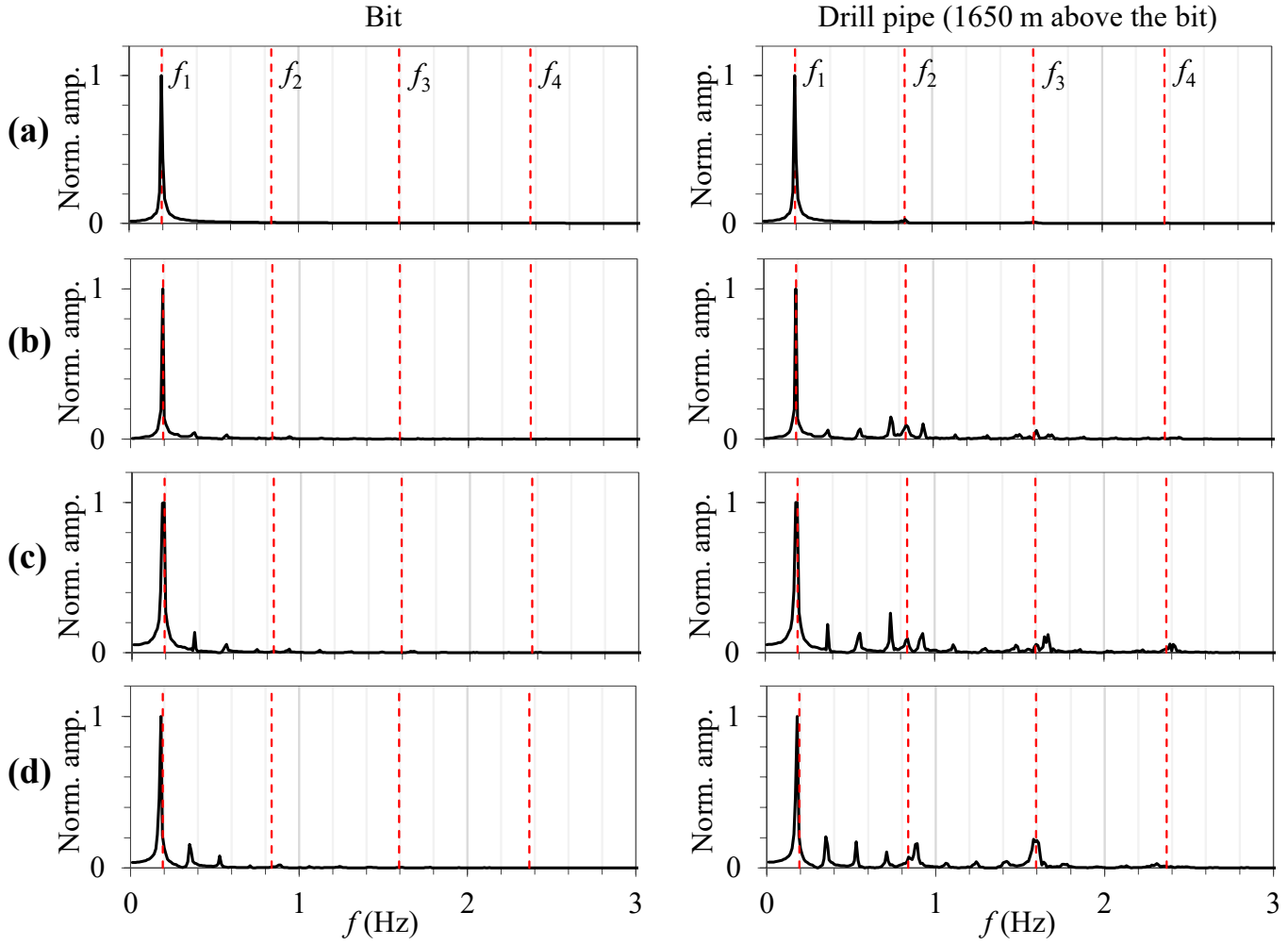

Figure 14. Response spectra of angular velocity at the drill bit (**left**) and 1650 m above the bit (**right**) for Ω_r = 6.3 rad/s, ξ = 0.03, and W_b of (**a**) 10 kN, (**b**) 30 kN, (**c**) 40 kN, and (**d**) 50 kN. Dashed lines indicate natural frequencies.

4.3. Effect of Damping Ratio ξ

To conduct a detailed investigation of the effect of mud damping on stick–slip vibration of the drill string, nine values of ξ were considered, as given in Table 6. For each ξ, the corresponding α and β were calculated using Equation (6) with ω_i = 1.2056 rad/s and ω_j = 44.2 rad/s. The Ω_r and W_b were fixed at 5.24 rad/s and 40 kN, respectively.

Table 6. ξ and the corresponding values for α and β.

ξ	α	β
	(1/s)	(s)
0.03	0.070416	0.00132142
0.05	0.117361	0.00220237
0.07	0.164305	0.00308332
0.10	0.234721	0.00440474
0.15	0.352082	0.00660711
0.20	0.469442	0.00880948
0.25	0.586803	0.01101185
0.27	0.633747	0.01189280
0.30	0.704164	0.01321422

Figures 12 and 13 illustrate the time series and phase planes of the angular velocity at the bit and a drill pipe located 1400 m above the bit, respectively, for different damping ratios. For ξ smaller than a certain value, i.e., 0.05, 0.10, and 0.20, the drill string responds with periodic torsional vibrations at the drill pipe and stick–slip at the drill bit; see plots (a)–(c) in Figures 15 and 16. It can be seen that increasing ξ decreases both the duration of the stick phase at the bit and the amplitude of the torsional vibration at the drill pipe and bit. For ξ higher than a particular threshold value, i.e., 0.27, the stick–slip vibration is removed, and thus, the angular velocities of the drill pipe and drill collars/bit come close to the rotary velocity; see plot (d) in Figures 15 and 16. The loss of stick–slip vibration above the threshold damping is in agreement with previous observations (e.g., [1,34,47]).

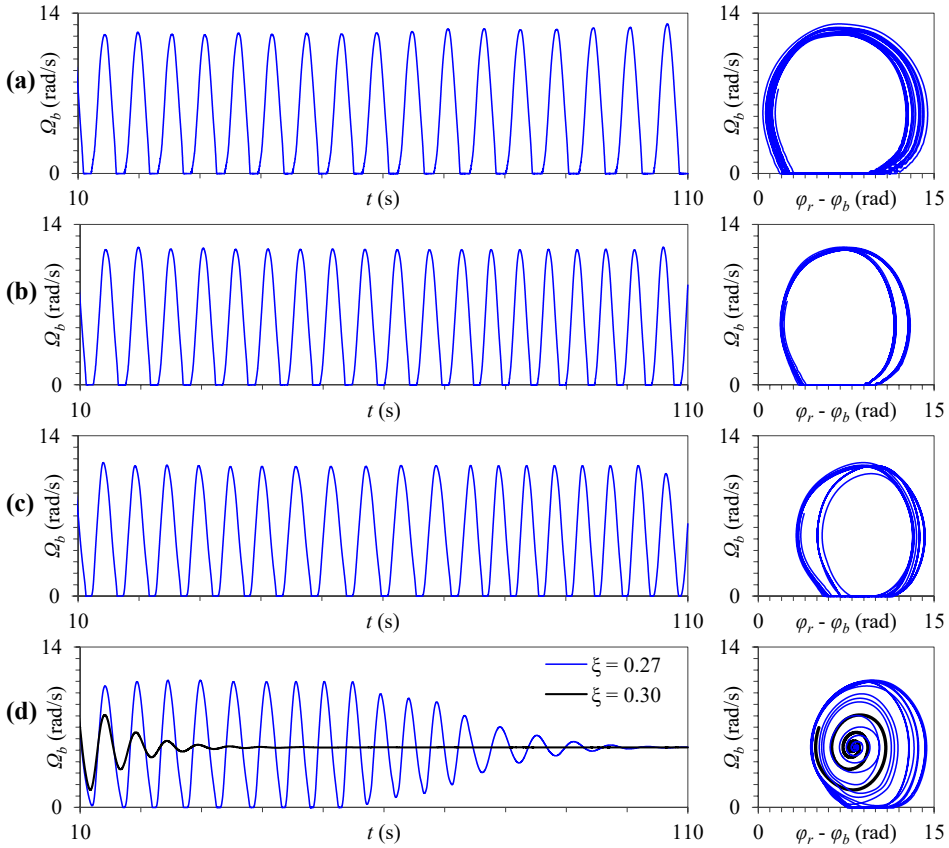

Figure 15. Time series and phase planes of the angular velocity at the bit for Ω_r = 5.24 rad/s, W_b = 40 kN, and ξ of (**a**) 0.05, (**b**) 0.10, (**c**) 0.20, (**d**) 0.27, and 0.30.

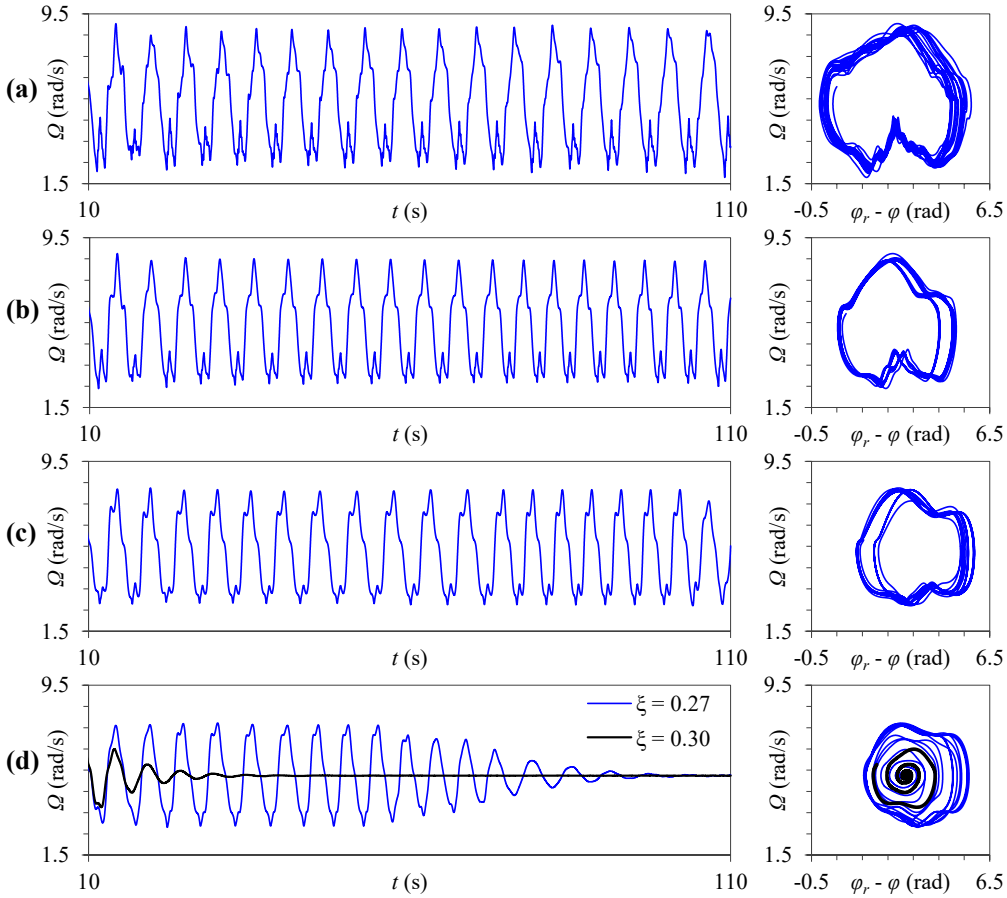

Figure 16. Time series and phase planes of the angular velocity at 1400 m above the bit for Ω_r = 5.24 rad/s, W_b = 40 kN, and ξ of (**a**) 0.05, (**b**) 0.10, (**c**) 0.20, (**d**) 0.27, and 0.30.

Table 7 shows the mean angular velocity along the drill string for different ξ. By increasing ξ, the mean angular velocity along the drill string does not change significantly and remains in the vicinity of Ω_r.

Table 7. Mean angular velocity (μ) at different points along the drill string for Ω_r = 5.24 rad/s, W_b = 40 kN, and varying ξ.

Distance Above the Bit (m)	ξ = 0.05	ξ = 0.10	ξ = 0.20	ξ = 0.27
2150	5.24	5.24	5.24	5.24
1900	5.23	5.23	5.23	5.24
1650	5.22	5.22	5.21	5.23
1400	5.21	5.21	5.20	5.23
1150	5.20	5.20	5.19	5.22
900	5.19	5.19	5.18	5.22
650	5.18	5.18	5.17	5.21
400	5.18	5.17	5.16	5.21
150	5.17	5.15	5.15	5.20
112.5	5.17	5.15	5.15	5.20
75	5.17	5.15	5.15	5.20
37.5	5.17	5.15	5.15	5.20
0	5.17	5.15	5.15	5.20

Figure 17 shows the response spectra of the angular velocities for varying ξ. According to this figure, the dominant frequency of the stick–slip vibration f_D = 0.18~0.19 Hz for varying ξ remains close to, i.e., slightly smaller than, the first natural torsional frequency of the system 0.19188 Hz. Although the influence of viscous mud damping on the dominant frequency might be negligible, it introduces a ragged behavior in the spectra.

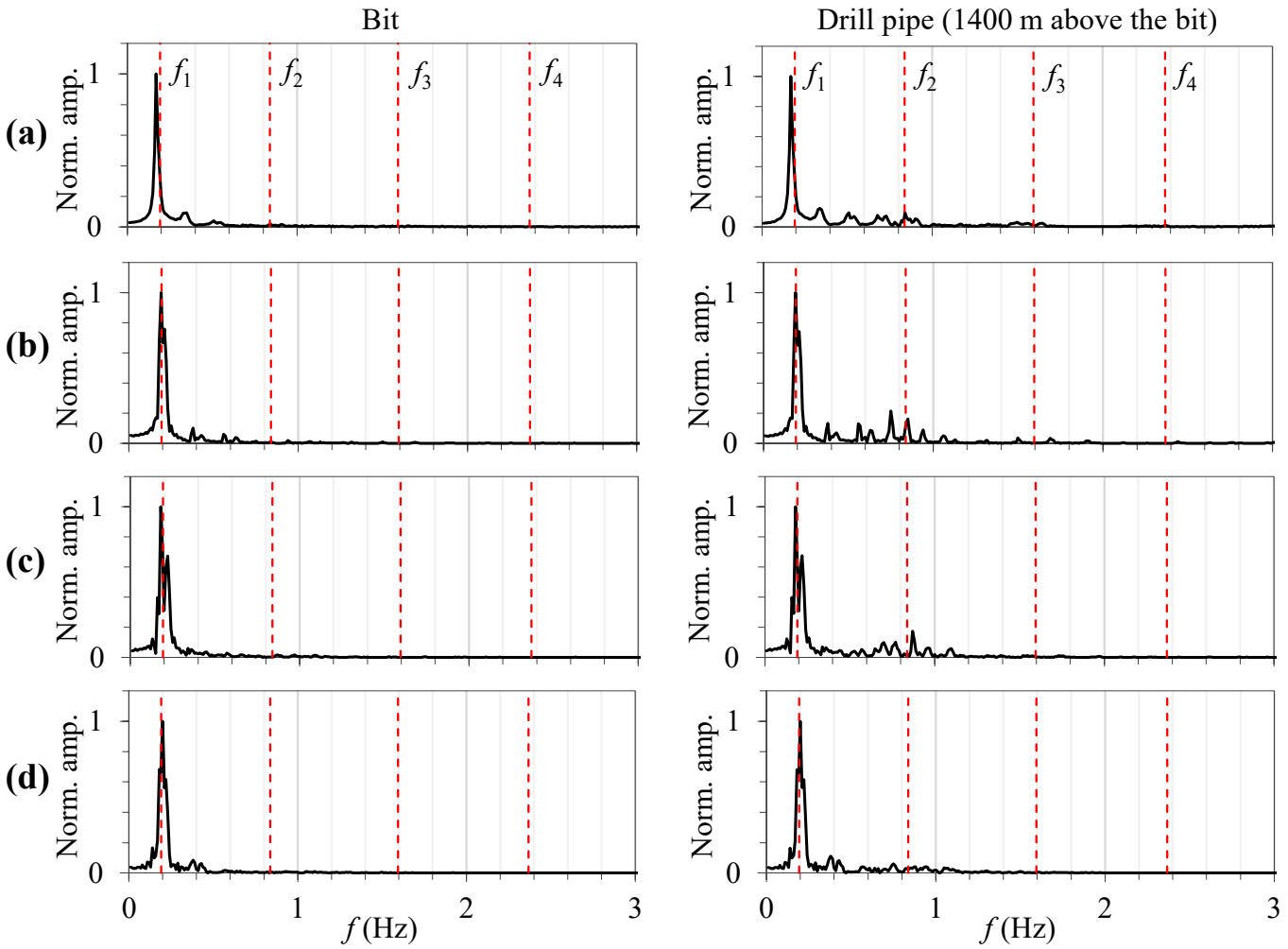

Figure 17. Response spectra of angular velocity at the drill bit (**left**) and 1400 m above the bit (**right**) for Ω_r = 5.24 rad/s, W_b = 40 kN, and ξ of (**a**) 0.05, (**b**) 0.10, (**c**) 0.20, and (**d**) 0.27.

The comparison between the stick–slip response predicted by the analytical and the numerical model when varying damping ratios showed a noticeable difference between their threshold damping values. Figure 18 demonstrates the result of the comparison. For ξ up to 0.10, both the lumped-parameter and FEM models predict a steady-state stick–slip vibration; see Figure 18a. By reaching ξ = 0.13, however, the stick–slip is eliminated in the lumped-parameter model, whereas the FEM model shows a continuous stick–slip oscillation; see Figure 18b. The difference in the threshold damping between the numerical and analytical models may be related to the Rayleigh damping model, which does not guarantee an equal value of the damping coefficient for all the vibration modes.

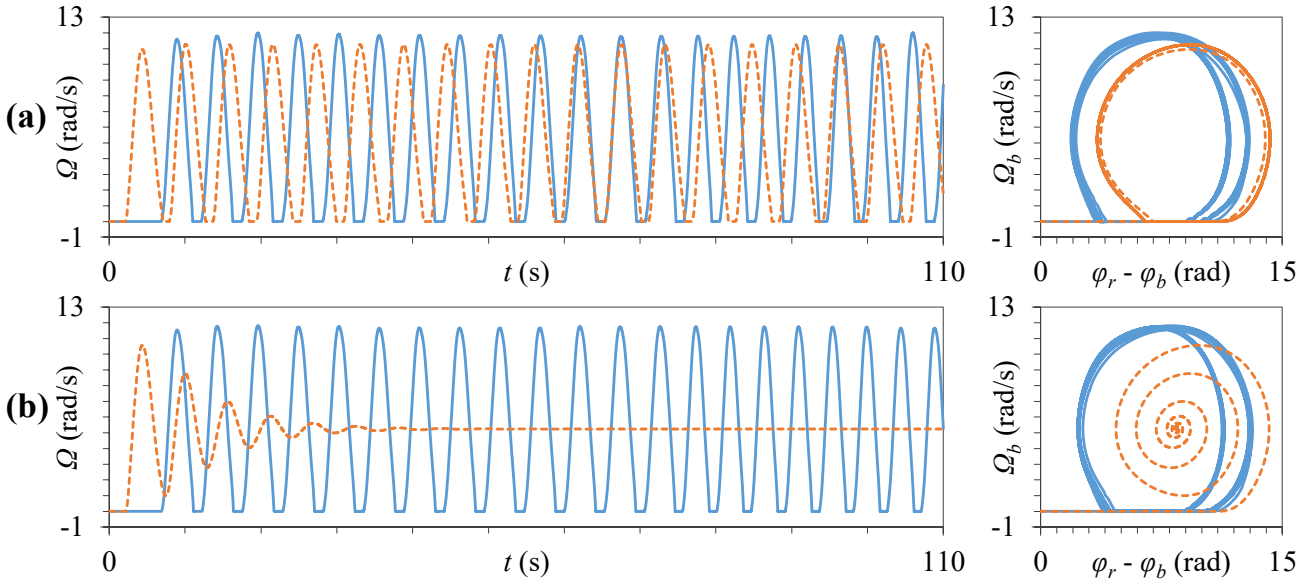

Figure 18. Time series (**left**) and phase planes (**right**) of the bit response obtained from the FEM model (solid lines) and the lumped-parameter model (dashed lines) for Ω_r = 5.24 rad/s, W_b = 40 kN, and ξ of (**a**) 0.10 and (**b**) 0.13.

4.4. System Behavior

To gain a better understanding of the dynamical behavior of the entire drill string, the variations of the amplitude and standard deviation of angular velocities along the drill string with Ω_r, W_b, and ξ are shown in Figures 19 and 20, respectively.

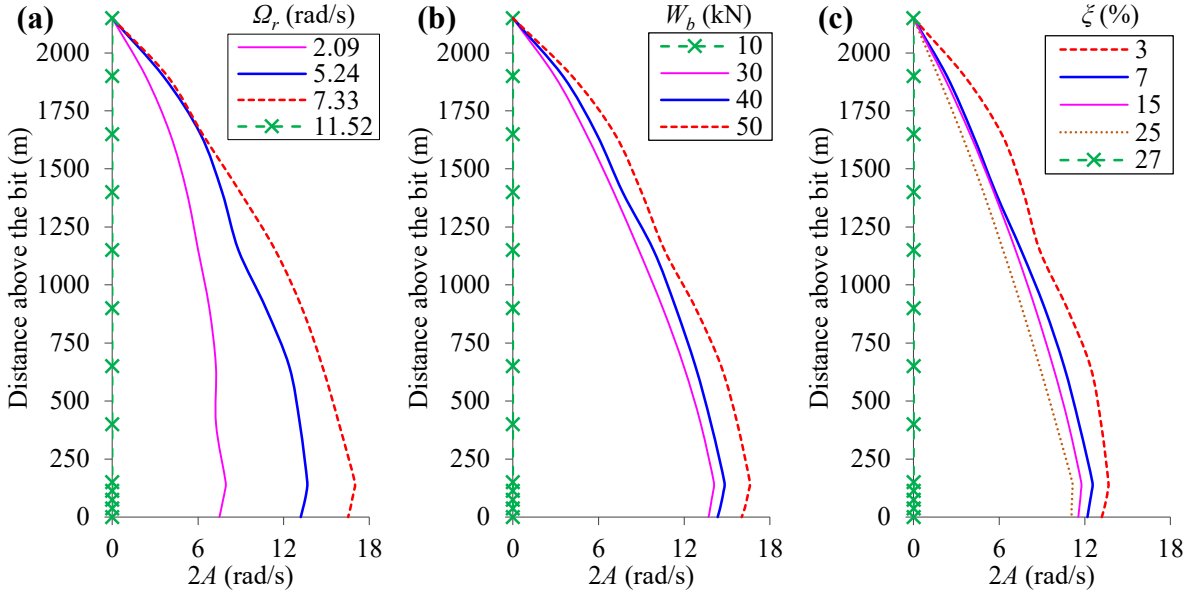

Figure 19. Variation of the peak-to-peak amplitude of angular velocity along the drill string under different stick–slip conditions. (**a**) W_b = 40 kN and ξ = 0.03, (**b**) Ω_r = 6.3 rad/s and ξ = 0.03, and (**c**) Ω_r = 5.24 rad/s and W_b = 40 kN.

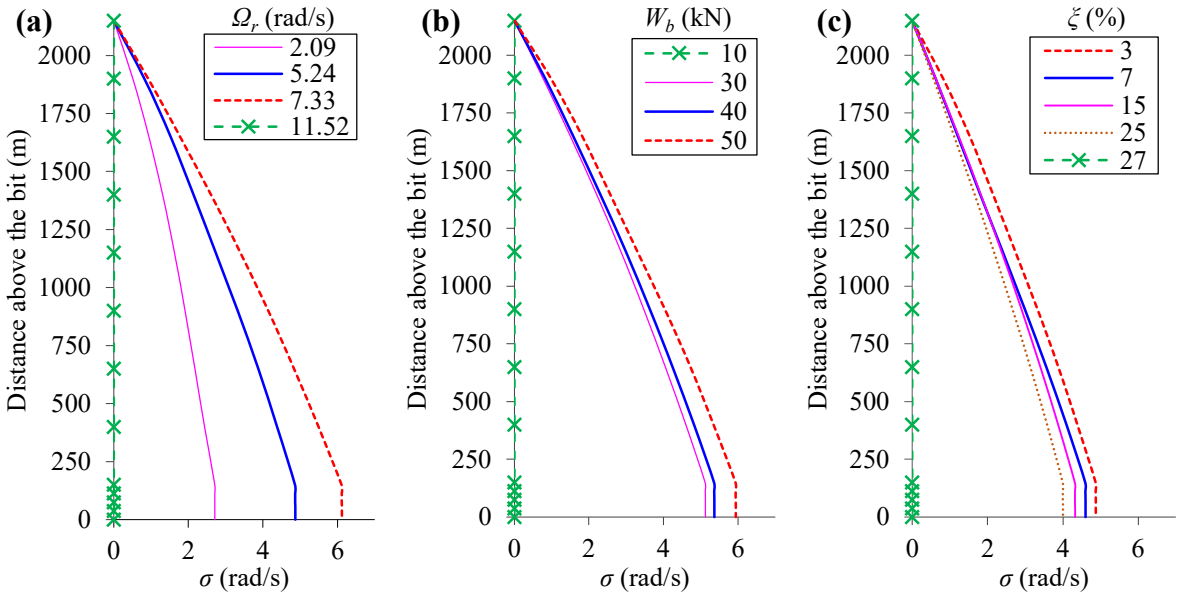

Figure 20. Variation of the standard deviation of angular velocity along the drill string under different stick–slip conditions. (**a**) W_b = 40 kN and ξ = 0.03, (**b**) Ω_r = 6.3 rad/s and ξ = 0.03, and (**c**) Ω_r = 5.24 rad/s and W_b = 40 kN.

Under each stick–slip condition, the vibration amplitude A and standard deviation σ along the drill string increase rapidly from zero at the rotary table to the maximum at the top of the drill collars and remain almost constant along the collar section. This shows that the torsional stick–slip oscillation of the drill collars/bit is more crucial than the drill pipes with regard to the intensity. The almost constant-amplitude torsional vibration along the drill collars is mainly due to the high torsional stiffness of the collar section, which makes it behave as a rigid body.

The amplitude and standard deviation of the angular velocity of the drill pipes and drill collars/bit along the drill string under stick–slip oscillation increase with Ω_r and W_b, as depicted in plots (a)–(b) in Figures 19 and 20, respectively, but decrease with ξ, as depicted in plot (c) in Figures 19 and 20. A Ω_r or ξ higher than a threshold value or a W_b lower than a threshold value can remove the stick–slip oscillations. As the stick–slip is removed, the amplitudes and standard deviations of the angular velocity of both the drill pipes and drill collars/bit reach zero. It is noted that although stick–slip vibration can be reduced or even eliminated by increasing the rotary velocity above the threshold value, the vibration amplitudes and standard deviations along the drill string can be intensified before reaching the threshold velocity; see plot (a) in Figures 19 and 20. This, in turn, can result in larger cyclic stresses in the drill pipes and drill collars, detrimental to the life of the system.

Varying the ξ does not significantly alter the stick–slip vibration; see plot (c) in Figures 19 and 20. For example, increasing the ξ from 0.07 to 0.10, which is an increase of 42.86%, decreases the standard deviation of the drill collar by only 3%. Similarly, increasing the ξ from 0.03 to 0.25, which is an increase of 833.33%, decreases the standard deviation of the drill collars/bit by 17.89%. Therefore, if Ω_r and W_b are to be kept constant, and the stick–slip is treated only by altering the viscous damping, then a large damping should be considered for mitigation. It is noted that although viscous damping can reduce the amplitude of torsional vibration along the drill string or even remove the stick–slip vibration, the realistic damping value may be too small to eliminate the oscillations at field operating conditions.

The growth of the amplitude of the torsional vibration at each point along the drill string with regard to the stick–slip is significantly affected by the rotary velocity rather than the weight-on-bit and viscous damping.

5. Summary and Conclusions

In this paper, based on mathematical and mechanical theories, a detailed numerical investigation of the drill string stick–slip motion was presented. Firstly, an efficient and robust nonlinear FE model was developed to predict the vibrations of the full drill string. The stick–slip phenomenon was efficiently modeled by incorporation of the highly nonlinear bit–rock interaction and the viscous mud-damping effect along the entire drill string. An alternative approach was proposed based on the rate-dependent behavior of the torque-on-bit that has been observed in the published data. The nonlinear Timoshenko beam (shear deformation) was implemented. The nonlinear effects of large rotational displacements, the geometrically nonlinear axial–torsional coupling effects, and the axial and torsional stiffness of the drill pipes and drill collars were considered in the model. A modal analysis was conducted to estimate the eigenfrequencies of the drill string system through a linear perturbation frequency analysis. A procedure was proposed to properly select the Rayleigh damping coefficients in order to minimize the variation of the frequency-dependent damping and retain the effect of higher vibration modes of the system. A nonlinear torsional lumped-parameter model of the full drill string was developed considering the dynamics of the drill pipes, drill collars, and drill bit, accounting for the bit–rock interaction and the equivalent mud damping. The accuracy of the developed FEM and lumped-parameter models was verified against the field test data.

Secondly, the influence of rotary velocity, weight-on-bit, and viscous mud damping on the system dynamics was investigated. Particular attention was paid to the torsional behavior of both the drill pipes and drill collars/bit rather than focusing only on the BHA response. The time series of angular velocities were obtained for different points along the drill string under each operating condition. The mean, peak-to-peak amplitude, and standard deviation of the obtained velocity time series under different operating conditions were computed and compared. Spectral analyses were carried out to determine the frequency components of the torsional vibration of the drill pipes and drill collars/bit.

The results showed that the mean angular velocity of each point along the drill string was directly related to the rotational velocity at the surface but independent of the weight-on-bit and damping ratio. Variation of rotary velocity was more influential with regard to the growth of the amplitude and standard deviation of stick–slip vibration at each point along the drill string compared to the weight-on-bit and damping ratio. The stick–slip dominant frequency was dependent mainly on the angular velocity of the rotary table and was decreased with decreasing the rotary velocity. Nevertheless, the dominant frequency appeared to be independent of the weight-on-bit and damping for the considered drill string and operating conditions. The contribution of higher frequencies to the torsional stick–slip response of the drill collars/bit was negligible. However, noticeable peaks were observed at frequencies close to the higher natural vibration modes of the system in the response spectra of the drill pipes under low rotary velocities. The intensity of the higher frequency components in the response of the drill pipes increased with decreasing the rotary velocity.

In summary, the study demonstrated new characteristics of the stick–slip motion of the entire drill string and provided the significant influence of the rotary table velocity on the self-excited torsional motions of the drill string.

Author Contributions: Conceptualization, M.J.M., H.S. and C.d.A.M.; methodology, M.J.M., H.S. and C.d.A.M.; software, H.S. and C.d.A.M.; validation, M.J.M.; formal analysis, M.J.M.; investigation, M.J.M.; resources, H.S. and C.d.A.M.; data curation, M.J.M.; writing—original draft preparation, M.J.M.; writing—review and editing, H.S. and C.d.A.M.; visualization, M.J.M.; supervision, H.S. and C.d.A.M.; project administration, H.S.; funding acquisition, H.S. All authors have read and agreed to the published version of the manuscript.

Funding: The authors gratefully acknowledge the financial support of this research by the Research and Development Corporation (RDC) (now IET) through the Ignite funding program, the visiting research funding by Mitacs through the Globalink program, and the Memorial University of Newfoundland through VP start-up funding support. Also, the first author gratefully acknowledges the Offshore Mechanics Laboratory (LMO) and the University of São Paulo for providing the visiting opportunity and collaboration.

Data Availability Statement: All of the data used in this study has been presented in the manuscript.

Conflicts of Interest: The authors declare no conflict of interest.

References

1. Jansen, J.D.; van den Steen, L. Active damping of self-excited torsional vibrations in oil well drillstrings. *J. Sound Vib.* **1995**, *179*, 647–668. [CrossRef]
2. MacDonald, K.A.; Bjune, J.V. Failure analysis of drill strings. *Eng. Fail. Anal.* **2007**, *14*, 1641–1666. [CrossRef]
3. Chevallier, A.M. Nonlinear Stochastic Drilling Vibrations. Ph.D. Thesis, Rice University, Houston, TX, USA, 2001. Available online: https://hdl.handle.net/1911/17946 (accessed on 10 July 2022).
4. Yigit, A.S.; Christoforou, A.P. Coupled torsional and bending vibrations of drillstrings subject to impact with friction. *J. Sound Vib.* **1998**, *215*, 167–181. [CrossRef]
5. Brett, J.F. The genesis of bit-induced torsional drillstring vibrations. *SPE Drill. Eng.* **1992**, *7*, 168–174. [CrossRef]
6. Christoforou, A.P.; Yigit, A.S. Fully coupled vibrations of actively controlled drillstrings. *J. Sound Vib.* **2003**, *267*, 1029–1045. [CrossRef]
7. Halsey, G.W.; Kyllingstad, A.; Kylling, A. Torque feedback used to cure slip-stick motion. In Proceedings of the SPE Annual Technical Conference and Exhibition, Houston, TX, USA, 5–8 October 1988. [CrossRef]
8. Chen, S.L.; Blackwood, K.; Lamine, E. Field investigation of the effects of stick-slip, lateral and whirl vibrations on roller-cone bit performance. *SPE Drill. Compl.* **2002**, *17*, 15–20. [CrossRef]
9. Khulief, Y.A.; Al-Sulaiman, F.A.; Bashmal, S. Vibration analysis of drillstrings with self-excited stick–slip oscillations. *J. Sound Vib.* **2007**, *299*, 540–558. [CrossRef]
10. Lin, Y.Q.; Wang, Y.H. Stick-slip vibration of drill strings. *ASME J. Eng. Ind.* **1991**, *113*, 38–43. [CrossRef]
11. Navarro-Lopez, E.M.; Cortes, D. Avoiding harmful oscillations in a drillstring through dynamical analysis. *J. Sound Vib.* **2007**, *307*, 152–171. [CrossRef]
12. Richard, T.; Germay, C.; Detournay, E. A simplified model to explore the root cause of stick-slip vibrations in drilling systems with drag bits. *J. Sound Vib.* **2007**, *305*, 432–456. [CrossRef]
13. Liu, X.; Vlajic, N.; Long, X.; Meng, G.; Balachandran, B. Nonlinear motions of a flexible rotor with a drill bit: Stick-slip and delay effects. *Nonlinear Dyn.* **2013**, *72*, 61–77. [CrossRef]
14. Kapitaniak, M.; Vaziri Hamaneh, V.; Páez Chávez, J.; Nandakumar, K.; Wiercigroch, M. Unveiling complexity of drill-string vibrations: Experiments and modelling. *Int. J. Mech. Sci.* **2015**, *101–102*, 324–337. [CrossRef]
15. Tang, L.; Zhu, X.; Shi, C.; Tang, J.; Xu, D. Study of the influences of rotary table speed on stick-slip vibration of the drilling system. *Petroleum* **2015**, *1*, 382–387. [CrossRef]
16. Tang, L.; Zhu, X. Effects of the Difference Between the Static and the Kinetic Friction Coefficients on a Drill String Vibration Linear Approach. *Arab. J. Sci. Eng.* **2015**, *40*, 3723–3729. [CrossRef]
17. Tang, L.; Zhu, X.; Qian, X.; Shi, C. Effects of weight on bit on torsional stick-slip vibration of oilwell drill string. *J. Mech. Sci. Technol.* **2017**, *31*, 4589–4597. [CrossRef]
18. Tucker, R.W.; Wang, C. An integrated model for drill-string dynamics. *J. Sound Vib.* **1999**, *224*, 123–165. [CrossRef]
19. Silveira, M. A Comprehensive Model of Drill-String Dynamics Using Cosserat Rod Theory. Ph.D. Thesis, University of Aberdeen, Aberdeen, UK, 2011. Available online: https://ethos.bl.uk/OrderDetails.do?uin=uk.bl.ethos.558596 (accessed on 15 May 2021).
20. Sampaio, R.; Piovan, M.T.; Lozano, G.V. Coupled axial/torsional vibrations of drill-strings by means of non-linear model. *J. Mech. Res. Commun.* **2007**, *34*, 497–502. [CrossRef]
21. Ritto, T.G.; Soize, C.; Sampaio, R. Non-linear dynamics of a drill–string with uncertain model of the bit–rock interaction. *Int. J. Non-Linear Mech.* **2009**, *44*, 865–876. [CrossRef]
22. Germay, C.; Denol, V.; Detournay, E. Multiple mode analysis of the self-excited vibrations of rotary drilling systems. *J. Sound Vib.* **2009**, *325*, 362–381. [CrossRef]
23. Dareing, D.W.; Livesay, B.J. Longitudinal and angular drill-string vibrations with damping. *ASME J. Eng. Ind.* **1968**, *90*, 671–679. [CrossRef]
24. Liao, C.M.; Vlajic, N.; Karki, H.; Balachandran, B. Parametric studies on drill-string motions. *Int. J. Mech. Sci.* **2012**, *54*, 260–268. [CrossRef]
25. Vlasov, V.Z. *Thin Walled Elastic Beams*, 2nd ed.; By the Israel Program for Scientific Translations; National Science Foundation: Washington, DC, USA, 1961.
26. *ABAQUS/Explicit User's Manual*; SIMULIA: Vélizy-Villacoublay, France, 2017.

27. Bradbury, R.E.; Wilhoit, J.C. Effect of tool joints on passages of plane longitudinal and torsional waves along a drill pipe. *ASME J. Eng. Ind.* **1963**, *85*, 156–162. [CrossRef]
28. Banerjee, A.K.; Dickens, J. Dynamics of an arbitrary flexible body in large rotation and translation. *J. Guid. Control Dyn.* **1990**, *13*, 221–227. [CrossRef]
29. Trindade, M.; Sampaio, R. Dynamics of beams undergoing large rotations accounting for arbitrary axial rotations. *J. Guid. Control Dyn.* **2002**, *25*, 634–643. [CrossRef]
30. Richard, T.; Detournay, E. Stick-slip vibrations of PDC bits. In Proceedings of the 4th North American Rock Mechanics Symposium, Seattle, DC, USA, 28 June–1 July 2009.
31. Pavone, D.R.; Desplans, J.P. Application of high sampling rate downhole measurements for analysis and cure of stick–slip in drilling. In Proceedings of the SPE Annual Technical Conference and Exhibition, New Orleans, LA, USA, 25–28 September 1994. [CrossRef]
32. Abbassian, F.; Dunayevsky, V.A. Application of stability approach to torsional and lateral bit dynamics. *SPE Drill. Compl.* **1998**, *13*, 99–107. [CrossRef]
33. Challamel, N.; Sellami, H.; Chenevez, E.; Gossuin, L. A stick-slip analysis based on rock/bit interaction: Theoretical and experimental contribution. In Proceedings of the IADC/SPE Drilling Conference, New Orleans, LA, USA, 23–25 February 2000. [CrossRef]
34. Dawson, R.; Lin, Y.Q.; Spanos, P.D. Drill-string stick-slip oscillations. In Proceedings of the SEM Spring Conference on Experimental Mechanics, Houston, TX, USA, 14–19 June 1987.
35. Kyllingstad, A.; Halsey, G.W. A study of slip/stick motion of the bit. *SPE Drill. Eng.* **1988**, *3*, 369–373. [CrossRef]
36. Zamanian, M.; Khadem, S.E.; Ghazavi, M.R. Stick-slip oscillations of drag bits by considering damping of drilling mud and active damping system. *J. Pet. Sci. Eng.* **2007**, *59*, 289–299. [CrossRef]
37. Nandakumar, K.; Wiercigroch, M. Stability analysis of a state dependent delayed, coupled two DOF model of drill-string vibration. *J. Sound Vib.* **2013**, *332*, 2575–2592. [CrossRef]
38. Liu, X.; Vlajic, N.; Long, X.; Meng, G.; Balachandran, B. Coupled axial-torsional dynamics in rotary drilling with state-dependent delay: Stability and control. *Nonlinear Dyn.* **2014**, *78*, 1891–1906. [CrossRef]
39. Bakhtiari-Nejad, F.; Hosseinzadeh, A. Nonlinear dynamic stability analysis of the coupled axial-torsional motion of the rotary drilling considering the effect of axial rigid–body dynamics. *Int. J. Non-Linear Mech.* **2017**, *88*, 85–96. [CrossRef]
40. Rayleigh, L. *Theory of Sound*; Dover: New York, NY, USA, 1945.
41. Chopra, A.K.; McKenna, F. Modeling viscous damping in nonlinear response history analysis of buildings for earthquake excitation. *Earthq. Eng. Struct. Dyn.* **2016**, *45*, 193–211. [CrossRef]
42. Nessjøen, P.J.; Kyllingstad, A.; Dambrosio, P.; Fonseca, I.S.; Garcia, A.; Levy, B. Field experience with an active stick-slip prevention system. In Proceedings of the SPE/IADC Drilling Conference and Exhibition, Amsterdam, The Netherlands, 1–3 March 2011. [CrossRef]
43. Karnopp, D. Computer simulation of stick–slip friction in mechanical dynamic systems. *ASME J. Dyn. Syst. Meas. Control.* **1985**, *107*, 100–103. [CrossRef]
44. Sepehri, N.; Sassani, F.; Lawrence, P.D.; Ghasempoor, A. Simulation and experimental studies of gear backlash and stick-slip friction in hydraulic excavator swing motion. *ASME J. Dyn. Syst. Meas. Control.* **1996**, *118*, 463–467. [CrossRef]
45. Leine, R.I.; van Campen, D.H.; de Kraker, A.; van den Steen, L. Stick-slip vibrations induced by alternate friction models. *Nonlinear Dyn.* **1998**, *16*, 41–54. [CrossRef]
46. Mihajlovic, N.; van Veggel, A.A.; van de Wouw, N.; Nijmeijer, H. Analysis of friction-induced limit cycling in an experimental drill-string system. *ASME J. Dyn. Syst. Meas. Control.* **2004**, *126*, 709–720. [CrossRef]
47. Kyllingstad, A.; Nessjøen, P.J. A New Stick-Slip Prevention System. *Soc. Pet. Eng.* **2009**. [CrossRef]
48. Moharrami, M.J.; Martins, C.A.; Shiri, H. Nonlinear integrated dynamic analysis of drill strings under stick-slip vibration. *Appl. Ocean Res.* **2021**, *108*, 102521. [CrossRef]
49. Liu, Y.; Páez Chávez, J.; De Sa, R.; Walker, S. Numerical and experimental studies of stick–slip oscillations in drill-strings. *Nonlinear Dyn.* **2017**, *90*, 2959–2978. [CrossRef]